J Porous Mater (2015) 22:843–850
DOI 10.1007/s10934-015-9957-1

An investigation into the crystallization of low-silica X zeolite

Lu Zhang[1] · **Yining Huang**[1]

Published online: 3 April 2015

Abstract The crystallization of low-silica X (LSX) zeolite with FAU topology was examined under hydrothermal synthesis conditions. PXRD was employed to follow the evolution of the long-range ordering of the gel. Raman spectra provided information on various ring and cage species existing in the gel. ^{27}Al and ^{29}Si solid-state NMR spectroscopy was utilized to monitor the change in local environment of tetrahedral sites. The results indicate that an amorphous aluminosilicate phase was formed immediately upon mixing different reactive species. Hydrothermal treatment led to the formation of sodalite-cage like species and the species with larger cavities, joint four-member rings (4Rs) and branched 4Rs, which are the structural building units of the FAU framework. These units were assembled into the crystalline structure of LSX zeolite. ^{23}Na and ^{39}K solid-state NMR results show that the transformation process was accompanied by the changes of the local structure of hydrated Na^+ and K^+ ions. The two types of cations may work synergistically to template the crystallization of LSX zeolite.

Keywords Zeolites · Faujasite · Crystallization · Hydrothermal synthesis · Solid-state NMR · Raman spectroscopy

✉ Yining Huang
yhuang@uwo.ca

[1] Department of Chemistry, The University of Western Ontario, London, ON N6A 5B7, Canada

1 Introduction

Zeolites are crystalline microporous aluminosilicates with three-dimensional framework formed by connecting SiO_4 and AlO_4 tetrahedra. There is a negative charge associated with every Al atom, which is balanced by an exchangeable cation, thus resulting in a neutral structure [1, 2]. Depending on their structures and compositions, zeolites have been widely used in industry as catalysts, adsorbents, and ion exchangers [3]. There are 225 types of zeolitic topologies identified [4], but only a limited number of them have exhibited practical applications [5]. Zeolites with faujasite (FAU) structure are one of the most important zeolitic materials.

The FAU framework (Scheme 1) consists of two interconnecting 3D networks of cavities with the larger ones (supercages) of a free diameter of about 13 Å and smaller ones (sodalite or β cages) of a free diameter of about 7 Å [6]. By virtue of Si content, faujasite zeolite is categorized into two kinds: zeolite X having a Si/Al atomic ratio ranging from 1.0 to 1.5 and zeolite Y having a Si/Al atomic ratio above 1.5 [7]. The application of faujasite zeolites in base-catalyzed reactions depends on their negatively charged framework. Alkali ion-exchanged faujasite zeolites exhibit basicity, and the basicity increases with decreasing Si/Al ratio due to the increased number of cations in the framework [8]. Low-silica X (LSX) zeolite has a Si/Al ratio of from 1.0 to about 1.1, and therefore, the maximum possible number of exchangeable cations [6, 9]. Due to its high extra-framework cation content, LSX zeolite is also one of the best sorbents in industry used for N_2/O_2 separation in air by adsorption processes [10, 11].

To date, much data has been obtained on the synthesis, characterization, and application of LSX zeolite [12–32]. Kühl has found that pure LSX zeolite can only be obtained

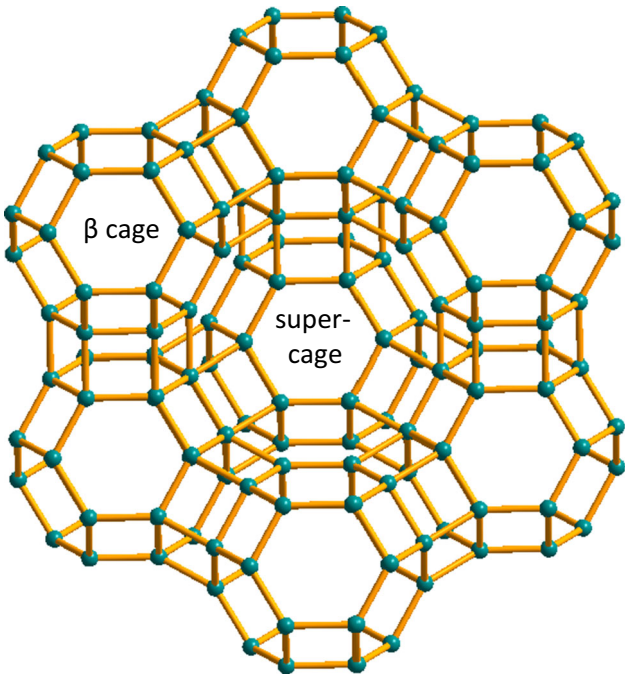

Scheme 1 Structure of the FAU framework

when the reaction mixture contains both sodium and potassium ions [33]. The K/(Na + K) ratio is a critical factor for the synthesis of LSX zeolite [34]. The growing applications of LSX zeolite require a better understanding of its nucleation and crystal growth process. Li et al. [35–37] previously took advantage of in situ and ex situ UV Raman techniques to probe the formation process of zeolite X (Si/Al atomic ratio is between 1.1 and 1.5). They proposed that the crystalline zeolite X framework was formed via the assembly of four-membered rings (4Rs) and 4R branched derivatives in the solid phase and monomeric silicate species in the liquid phase. Later Depla et al. [38] carried out in situ studies of the crystallization of LSX zeolite by simultaneous UV Raman and X-ray diffraction (XRD) measurements. They pointed out the existence of 4Rs and 6Rs in the amorphous gel at an early stage of crystallization. By adding K^+ ions into the synthetic solution, Iwama et al. [34] proposed that K^+ ions play a strong salting-out effect during the formation of LSX zeolite and prevent aluminosilicate precursors from assembling into zeolite A (LTA framework, also composed of sodalite cages connected by double 4Rs). In spite of much progress in studying the self-assembly process of LSX zeolite, detailed knowledge of its crystallization process is still lacking. For instance, Na^+ and K^+ ions are considered to play a structure-directing role in the formation of many zeolites [39]. The chemical environments of the two types of cations during the crystallization of LSX zeolite, however, have not been studied. Here, we report our recent work on the investigations of the crystallization of LSX zeolite. Relations between the structures of the intermediates and the local environments of ^{27}Al, ^{29}Si, ^{23}Na, and ^{39}K nuclei were probed by solid-state NMR spectroscopy in combination with other characterization techniques such as powder XRD and Raman spectroscopy.

2 Experimental

2.1 Sample preparation

LSX zeolites were synthesized by using the method reported by Kühl [33]. The reagents were sodium aluminate (Strem Chemicals, ca. 92 wt% $NaAlO_2$), sodium hydroxide (Caledon Laboratory Chemicals, ca. 97 wt%), potassium hydroxide (BDH, ca. 85 wt%), and sodium silicate (Aldrich, ca. 7 wt% Na_2O and 27 wt% SiO_2). The initial gel composition was 5.5 Na_2O:1.65 K_2O:1.0 Al_2O_3:2.2 SiO_2:122 H_2O.

A typical procedure for hydrothermal synthesis of LSX zeolite gel samples was the following: 13.0 g potassium hydroxide, 8.7 g sodium hydroxide, and 34.4 g water were combined and subjected to vigorous stirring for 10 min. Separately, 7.2 g sodium aluminate and 20.4 g water were mixed and added to the former mixture after being stirred for 5 min. Subsequently, a mixture of 19.6 g sodium silicate and 20 g water was added. The final solution was first stirred at room temperature for 10 min and then transferred into several polypropylene bottles, which were capped and sealed with paraffin films (referred to as the initial gel). After static aging in an oven at 343 K for 3 h, crystallization was carried out at 373 K for different times. The bottles were taken out of the oven and quenched in cold water after specified lengths of time. The product in each autoclave was filtered and the solid phase was washed by using 0.01 M sodium hydroxide instead of water to avoid over washing and hydrolysis [32]. The solid materials which are intermediates were then dried in air at room temperature and kept in tightly sealed glass vials for analysis.

2.2 Characterization

PXRD patterns were recorded on a Rigaku diffractometer using Co Kα radiation ($\lambda = 1.7902$ Å). Raman experiments were carried out with a customized Raman microspectroscopy system. A 514 nm line produced from an Ar^+ laser (Coherent Inc.) was used as the excitation source. The resolution was 0.1 cm^{-1}.

The NMR experiments were carried out on a Varian/Chemagnetics Infinityplus 400 WB spectrometer equipped with three rf channels operating at the field strength of 9.4 T. The Larmor frequencies of ^{1}H, ^{23}Na, ^{27}Al, and ^{29}Si were 399.5, 105.7, 104.1, and 79.4 MHz, respectively. The chemical shifts of ^{23}Na, ^{27}Al, and ^{29}Si were referenced to 1 M NaCl (0 ppm), 1 M $Al(NO_3)_3$ (0 ppm), and tetrakis(trimethylsilyl)-silane ($SiMe_3$, −9.9 ppm with respect to liquid tetramethylsilane) [40]. Depending on the requirements of individual experiment, three MAS probes were used (a Varian/Chemagnetics 7.5 mm, a 4.0 mm H/X/Y triple-tuned T3 MAS, and a 5.0 mm H/F/X/Y triple-tuned MAS probe). Both the ^{23}Na and ^{27}Al MAS spectra were acquired using a very small pulse angle with a pulse delay of 1 s. For the ^{29}Si MAS experiments, a 45° pulse was used with a pulse delay of 60 s.

For selected LSX intermediate gel samples, ^{39}K NMR experiments were carried out at 21.1 T on a Bruker Advance-900 spectrometer at the National Ultrahigh-Field NMR Facility for Solids in Ottawa, Canada. The Larmor frequency of ^{39}K is 42.0 MHz. The chemical shift was referenced to 1.0 M KCl (aq) in H_2O. The spectra were acquired using a 7.5-mm H/X MAS Bruker probe with a spinning speed of 5 kHz. ^{39}K NMR parameters, including C_Q, η_Q, and δ_{iso}, were determined by analytical simulations of NMR spectra using the WSOLIDS simulation package [41]. The experimental error for each measured parameter was determined by visual comparison of experimental spectra with simulations. The parameter of concern was varied bidirectionally starting from the best-fit value and all other parameters were kept constant, until noticeable differences between the spectra were observed.

3 Results and discussion

Figure 1 shows the powder XRD patterns of LSX gel samples recorded as a function of crystallization time. For the initial gel and samples heated for <3.2 h, all of the powder XRD patterns look identical and only contain a broad signal in the middle 2θ angle range, suggesting the amorphous nature of these solid samples. After heating the initial gel for 3.3 h, the corresponding XRD pattern shows several very weak reflection peaks whose positions coincide with the reflections of pure crystalline LSX zeolite [42]. This indicates that part of the amorphous phase has evolved into microporous FAU framework. Upon heating the gel for 3.5 h or longer, pure LSX zeolite with high crystallinity was yielded.

Based on vibrational motions of zeolite framework, Raman spectroscopy can provide structural information regarding ring sizes present in the intermediates [43, 44]. Therefore, it was used to monitor the development of pore openings during the formation process of LSX zeolite in this study (Fig. 2). The Raman spectra of zeolite X (Si/Al ratio is above 1.1) were previously reported by Li et al. [35, 36]. As zeolites LSX and X have the same framework topology, the assignments of the Raman bands were made mainly on the basis of their work. The bands at 500, 575, and 850 cm^{-1} in the initial gel, which are not characteristic Raman signals of LSX zeolite, suggest the presence of four-membered rings (4Rs) and 4R structures with branched chains (see Scheme 2 for illustrations). The bands observed at 1024 and 1060 cm^{-1} can be attributed to the T–O–T (T = Si, Al) asymmetric stretching mode [45, 46]. Further, the band at 1060 cm^{-1} may also result from

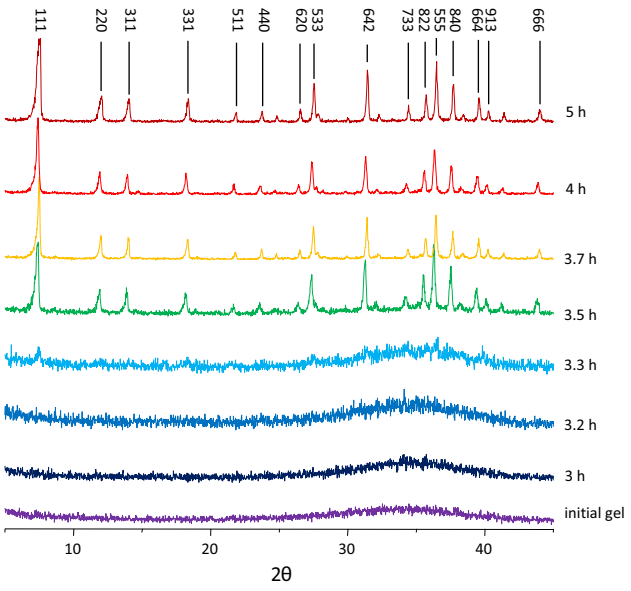

Fig. 1 Powder XRD patterns of LSX gel samples

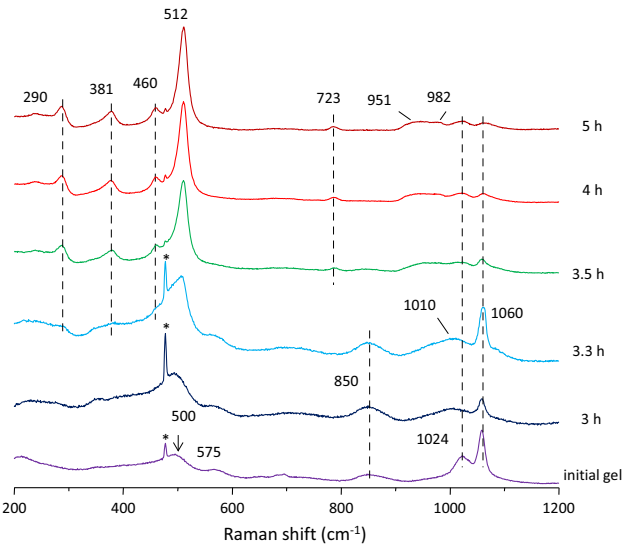

Fig. 2 Raman spectra of selected LSX gel samples. The *asterisk* is due to the background signal from glass slide

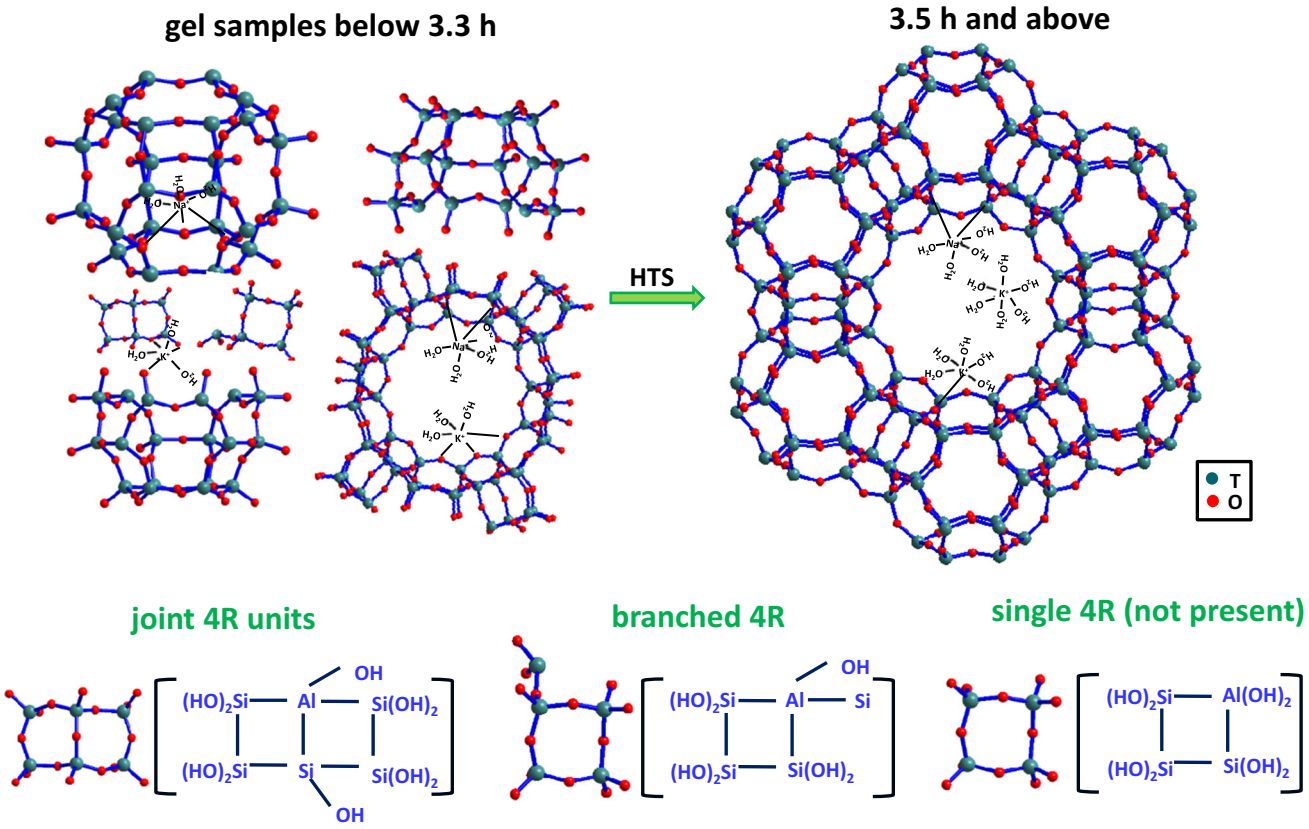

Scheme 2 An illustration of crystallization process of LSX zeolite and possible species in the gel

CO_3^{2-} formed by the reaction of excess NaOH in the initial gel with ambient CO_2. Its presence, however, has no influence in other species in the gel [47].

After 3 h of heating under hydrothermal conditions, a broad band at 1010 cm^{-1} became visible. This band was also present in the initial gel, but buried under the 1024 cm^{-1} signal. Observing this band is indicative of presence the species such as sodalite cages [35, 36]. This result suggests that few complete or nearly complete sodalite cages were formed immediately when aluminum and silicon sources were mixed together. After heating the initial gel for 3.3 h, the broad band at 500 cm^{-1} became sharper and shifted to 512 cm^{-1}, and this band is characteristic of the 4R breathing vibration mode for crystalline LSX zeolite. Further, two new weak bands at 290 and 381 cm^{-1}, which are assigned to the bending mode of double six-membered rings (D6Rs) [48] appeared. The band at 460 cm^{-1} results from the deformation of the T–O–T angle of 4Rs adjacent to K^+ ions [38]. These changes indicate that sodalite cages were connected via D6Rs to form crystalline LSX zeolite. Agreeing with the powder XRD pattern, this reveals the beginning of the crystallization. Upon heating the gel for 3.5 h or longer, the Raman bands remained unchanged. They are identical to the Raman signatures of the LSX framework [38]. The new band at 723 cm^{-1} is due to the symmetric T–O stretches [38]. The intensities of the bands at 1024 and 1060 cm^{-1} decreased a lot and two new bands at 951 and 982 cm^{-1} appeared, all of which are assigned to the asymmetric T–O stretches of TO_4 units [49]. The band between 900 and 1250 cm^{-1} is very sensitive to the Si/Al ratio of the zeolite framework [49]. The presence of the four bands in this region suggests that the as-synthesized FAU framework has the Si/Al ratio of around 1 [49], which is consistent with our ^{29}Si magic-angle spinning (MAS) NMR results (see discussions below). Further, the band at 575 cm^{-1} appeared at the very beginning of the crystallization process and then disappeared when the bands at 290 and 381 cm^{-1} appeared (3.5 h sample). This suggests that the branched 4Rs were closely related to the formation of D6Rs, and that the latter was formed from the assembly of the former [36].

Raman spectra indicate that small fragments existed during the crystallization of LSX. Indeed, the crystallization process of a microporous material can be described as the self-assembly process of the small fragments. Recently, Yan, Xu and co-coworkers identified the small fragments formed in the crystallization of aluminophosphate

molecular sieves by using solid-state NMR and the theoretical calculation [50, 51]. Thus, to further understand the structures of possible small fragments formed during the crystallization of LSX, we carried out solid-state NMR measurements. ^{27}Al MAS experiments were first performed to characterize the local environments of Al atoms in the intermediate phases (Fig. 3a). The spectra of the initial gel and the gel samples heated for <3.3 h exhibit a broad signal centered at around 59 ppm. This indicates the absence of $Al(OSi)_2(OH)_2$ species in the samples, which gives a signal at around 70 ppm [52]. This peak can be attributed to $Al(OSi)_3(OH)$ or $Al(OSi)_4$ species in amorphous aluminosilicate phase [52]. This result suggests that individual 4Rs containing only $Al(OSi)_2(OH)_2$ species were not present in these samples. A reasonable explanation is that complete or nearly complete sodalite cages and other 4R units such as joint 4R units and branched 4Rs were formed [53], as only $Al(OSi)_3(OH)$ and/or $Al(OSi)_4$ species exists in these structures. The formation of these structures agrees with the Raman spectra that show bands at 1010 (sodalite cages), 500 (joint 4R units), and 575 (branched 4Rs) cm^{-1}. The passible structures of these species are illustrated in Scheme 2. Heating the initial gel for 3.5 h or longer resulted in a sharper peak at 61 ppm. The corresponding powder XRD patterns and Raman spectra show the formation of crystalline LSX zeolite. This ^{27}Al signal is due to $Al(OSi)_4$ species with the high local Al ordering beyond the second coordination sphere in the crystalline zeolite framework.

^{29}Si MAS spectra were obtained to examine the short-range ordering around Si atoms during crystallization (Fig. 3b). The spectra of the initial gel and the gel samples heated for <3.3 h show a broad envelop at around −84 ppm. In the deconvoluted spectra, besides the major signal at −84 ppm, several other peaks at −80, −90, and −95 ppm coexisted. They can be attributed to $(AlO)_3SiOH$ or $(SiO)(AlO)Si(OH)_2$ (−84 ppm), $(AlO)_2Si(OH)_2$ (−80 ppm), $(SiO)_2Si(OH)_2$ (−90 ppm), and $(SiO)_2(AlO)SiOH$ (−95 ppm) species, respectively [54–56]. Together with the ^{27}Al NMR results, this observation supports the presence of joint 4R units in these samples. Heating the initial gel for 3.5 h or longer resulted in a sharp peak at −84 ppm and a much weaker one at −89 ppm. They can be ascribed to $Si(OAl)_4$ and $(SiO)_1Si(OAl)_3$ species in LSX zeolite [57].

The Si/Al ratio of zeolite framework can be calculated accurately from the relative intensities of different ^{29}Si signals [58]. A Si/Al ratio of 1.03 for LSX zeolite is obtained from the ^{29}Si MAS spectrum of 5 h sample. The elemental composition obtained from the Raman spectrum and the ^{29}Si MAS spectrum agrees with each other very well, both suggesting that the as-synthesized LSX zeolite has the Si/Al ratio of around 1.

^{23}Na MAS NMR spectroscopy has proven to be a powerful tool to determine cation distribution in hydrated and dehydrated zeolites [59]. Located at different crystallographic sites, Na^+ ions exhibit NMR signals with different chemical shifts. Thus, ^{23}Na MAS spectra were acquired to investigate the evolution of the local chemical environments of Na^+ ions as a function of crystallization time (Fig. 4).

For the initial gel and the gel samples heated below 3.2 h, the spectra contain a broad and asymmetric resonance at −6 ppm. The deconvoluted spectra indicate that

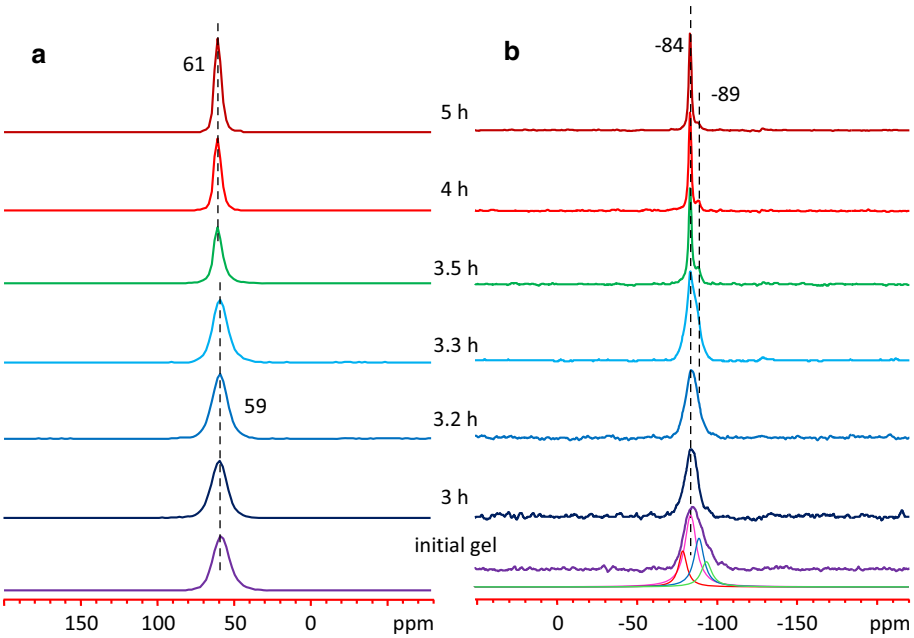

Fig. 3 ^{27}Al MAS (**a**) spectra and ^{29}Si MAS (**b**) spectra of selected LSX gel samples at 9.4 T

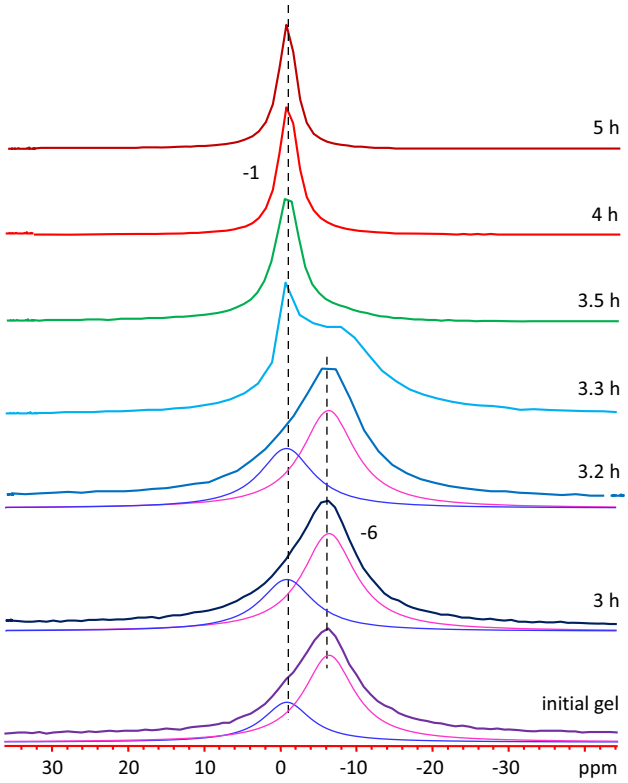

Fig. 4 ^{23}Na MAS spectra of selected LSX gel samples at 9.4 T

besides the −6 ppm peak, there is another weaker one at −1 ppm. In crystalline hydrated FAU zeolite, the −6 and −1 ppm resonance lines are assigned to hydrated Na^+ ions in the sodalite cage and supercage cage, respectively [7, 60, 61]. The −6 ppm signal in the gel samples below 3.2 h indicates that the cavities similar to sodalite cages may be formed. This agrees with the Raman and ^{27}Al NMR results. The −1 ppm signal suggests that another type of large cavities, which may result from the assembly of sodalite cages, joint 4Rs, and branched 4Rs, exists in these gel samples. The shift value close to zero indicates that highly hydrated Na^+ ions may give rise to this signal. Its broadness suggests that the cations probably sat in the large cavities that were randomly distributed. Thus, the gel samples obtained at an early stage of the crystallization likely contain sodalite cages and large cavities (Scheme 2). Upon heating the initial gel for 3.3 h, the −1 ppm signal became more prominent. The corresponding powder XRD pattern shows the appearance of several weak reflection peaks due to the FAU structure, and the Raman spectrum shows the formation of D6Rs. At this stage, it can be considered that the supercages were formed. Sodalite cages were connected with each other by D6Rs to form supercages. Upon further heating, the −1 ppm peak grew at the expense of the −6 ppm one and the −1 ppm peak is the only resonance observed in the final product (5 h sample). This reveals that under hydrothermal treatment, more supercages were formed from the reorganization of the above-mentioned structures. Further, this signal was much narrower, suggesting that highly hydrated Na^+ ions were located in a more uniform environment, which was supercage.

There are few solid-state ^{39}K NMR applications because of difficulties in obtaining NMR spectra, as the two NMR-active isotopes of potassium, ^{39}K and ^{41}K (natural abundance of 93.7 and 6.3 %, respectively), are spin-*3/2* quadrupolar nuclei with low magnetogyric ratios [62]. To investigate the role played by K^+ ions, ^{39}K MAS NMR experiments were carried out on selected gel samples at a magnetic field of 9.4 T at first. Unfortunately, no signals were observed due to the low sensitivity and broad resonances. To overcome the unfavorable properties of ^{39}K, the experiments were then performed at 21.1 T (Fig. 5). The spectral simulation results of the ^{39}K spectra are presented in Table 1.

In 5 h sample, a sharp peak centered at −1 ppm is present. The shift of this peak is close to that (−9 ppm) of hydrated potassium gallium silicate inorganic polymers reported in the literature [63]. This suggests that K^+ ions in as-made LSX were highly hydrated. The spectral simulation reveals a small C_Q value (0.7 MHz), indicating a highly spherically symmetric local environment around K^+ ions. Thus, the sharp signal at around −1 ppm signal in 5 h sample likely originates from the highly hydrated K^+ ions

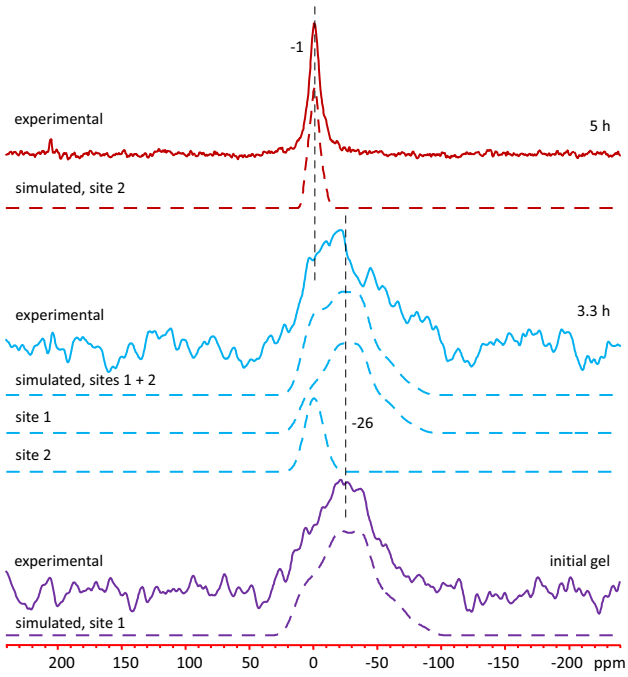

Fig. 5 ^{39}K MAS spectra of selected LSX gel samples at 21.1 T

Table 1 ^{39}K NMR parameters obtained from the simulation of ^{39}K NMR spectra

Samples	Sites	C_Q (MHz)	η_Q	δ_{iso} (ppm)
Initial gel	1	1.70 (2)	0.60 (2)	18 (1)
3.3 h	1	1.60 (2)	0.60 (2)	13 (1)
	2	0.70 (2)	0.75 (2)	7.3 (2)
5 h	2	0.70 (2)	0.75 (2)	7.3 (2)

located inside the supercages, where a large number of water molecules exist.

Different from that of 5 h sample, the spectrum of the initial gel exhibits a much broader quadrupolar powder pattern with a maximum at around −26 ppm. The simulation indicates that the isotropic chemical shift of this resonance is 18 ppm (Table 1). This value falls between −1 ppm for highly hydrated K^+ ions and 97 ppm for highly dehydrated K^+ ions in potassium aluminosilicate inorganic polymers [64]. The signal seen in the spectrum of the initial gel, therefore, is tentatively assigned to partially hydrated K^+ ions [65]. Further, despite of its broadness, it is not a featureless signal. It shows a lineshape due to second-order quadrupolar interaction and can be simulated using a single site (Fig. 5; Table 1). The C_Q value is 1.7 MHz, larger than 0.7 MHz due to highly hydrated K^+ ions in the product. This signifies that the local environment of partially hydrated K^+ ions in the initial gel, to a certain degree, had short-range ordering. These partially hydrated K^+ ions may sit within the large cavities or outside the complete or nearly complete sodalite cages, as suggested by the ^{23}Na NMR results. They may be coordinated to both water molecules and oxygen atoms of 4R structures or sodalite cages. Upon heating the initial gel for 3.3 h, In addition to the same broad signal seen in the initial gel, a shoulder at around −1 ppm appeared in the spectrum. Seeing the −1 ppm peak that is observed in the final LSX zeolite suggests the formation of supercages resulting from that some partially hydrated K^+ ions moved into the supercages. This result agrees with the ^{23}Na NMR results presented earlier. Further, the Raman spectrum of 3.3 h sample presents a 460 cm^{-1} band due to the interactions between K^+ ions and 4Rs [37]. The appearance of the −1 ppm signal thus suggests that partially hydrated K^+ ions organized the assembly of these 4R structures and large cavities into supercages and then became more hydrated.

4 Conclusions

At the very beginning of the synthesis process when different reactive species were mixed together, the initial gel contains amorphous aluminosilicate species with nearly complete sodalite cages, large cavities, joint 4Rs, and branched 4Rs. Upon heating under hydrothermal conditions, D6Rs were formed, resulting from the connection of joint 4Rs and branched 4Rs. They were assembled with sodalite cages or large cavities to form the crystalline framework of LSX zeolite. An illustration of the crystallization process of LSX zeolite is shown in Scheme 2. ^{23}Na and ^{39}K NMR results indicate that the degree of cation hydration as well as the local environments of Na^+ and K^+ ions changed during the crystallization and such changes accompanied the transformation process above. The two types of cations may work together to template the assembly process of LSX zeolite.

Acknowledgments Y. H. thanks the Natural Science and Engineering Research Council of Canada for a Discovery grant. Access to the 900 MHz NMR spectrometer was provided by the Canadian National Ultrahigh Field NMR Facility for Solids (http://nmr900.ca). We thank Dr. V. Terskikh for acquiring ^{39}K NMR spectra and Mr. P. He for ^{39}K spectral simulation. We also thank Prof. Yang Song for the access of a Raman spectrometer. This work was funded by the Natural Science and Engineering Research Council of Canada (2012).

Conflict of interest The authors declare that they have no conflict of interest.

References

1. R.J. Davis, J. Catal. **216**, 396 (2003)
2. R.A. Schoonheydt, P. Geerlings, E.A. Pidko, R.A. van Santen, J. Mater. Chem. **22**, 18705 (2012)
3. B. Smit, T.L.M. Maesen, Chem. Rev. **108**, 4125 (2008)
4. Ch. Baerlocher, L.B. McCusker, Database of zeolite structures. http://www.iza-structure.org/databases/
5. L. Zhang, A.N.C. Laak, P.E. Jongh, K.P. Jong, Microporous Mesoporous Mater. **126**, 115 (2009)
6. Y. Lee, S.W. Carr, J.B. Parise, Chem. Mater. **10**, 2561 (1998)
7. T. Frising, P. Leflaive, Microporous Mesoporous Mater. **114**, 27 (2008)
8. P. Kovacheva, K. Arishtirova, A. Predoeva, React. Kinet. Catal. Lett. **79**, 149 (2003)
9. A.F. Ojo, F.R. Fitch, M. Bülow, C.S. Gittleman, S.R. Jale, US Patent 6596256 (2003)
10. R.T. Yang, N.D. Hutson, US Patent 6780806 (2004)
11. R. Jasra, N. Choudary, S. Bhat, Ind. Eng. Chem. Res. **35**, 4221 (1996)
12. E. Basaldella, J. Tara, Zeolites **15**, 243 (1995)
13. G. Vitale, L.M. Bull, R.E. Morris, A.K. Cheetham, B.H. Toby, C.G. Coe, J.E. MacDougall, J. Phys. Chem. **99**, 16087 (1995)
14. D. Schaefer, D. Favre, M. Wilhelm, S. Weigel, B.J. Chmelka, Am. Chem. Soc. **119**, 9252 (1997)
15. J. Plevert, F. Di Renzo, F. Fajula, G. Chiari, J. Phys. Chem. B **101**, 10340 (1997)
16. M. Feuerstein, G. Engelhardt, P. McDaniel, J. MacDougall, T. Gaffney, Microporous Mesoporous Mater. **26**, 27 (1998)
17. S.R. Jale, M. Büow, F.R. Fitch, N. Perelman, D. Shen, J. Phys. Chem. B **104**, 5272 (2000)
18. US Patent, 6, 264, 881
19. S. Caldarelli, A. Buchholz, M. Hunger, J. Am. Chem. Soc. **123**, 7118 (2001)

20. J. Plévert, T. Okubo, Y. Wada, M. O'Keeffe, T. Tatsumi, Chem. Commun. **20**, 2112 (2001)
21. V.B. Kazansky, M. Bülow, E. Tichomirova, Adsorption **7**, 291 (2001)
22. D. Shen, M. Bülow, S.R. Jale, F.R. Fitch, A.F. Ojo, Microporous Mesoporous Mater. **48**, 211 (2001)
23. T. Loeser, D. Freude, G.T.P. Mabande, W. Schwieger, Chem. Phys. Lett. **370**, 32 (2003)
24. J.C. Buhl, M. Gerstmann, W. Lutz, A.Z. Ritzmann, Anorg. Allg. Chem. **630**, 604 (2004)
25. M. Romero, J. Gomez, G. Ovejero, A. Rodriguez, Mater. Res. Bull. **39**, 389 (2004)
26. J.E. Readman, C.P. Grey, M. Ziliox, L.M. Bull, A. Samoson, Solid State Nucl. Magn. Reson. **26**, 153 (2004)
27. V.B. Kazansky, N.A. Sokolova, M. Bülow, Microporous Mesoporous Mater. **67**, 283 (2004)
28. N. Sokolova, V. Kazanskii, Kinet. Catal. **46**, 879 (2005)
29. P. Khemthong, J. Wittayakun, S. Prayoonpokarach, Suranaree J. Sci. Technol. **14**, 367 (2007)
30. A. Wozniak, B. Marler, K. Angermund, H. Gies, Chem. Mater. **20**, 5968 (2008)
31. D. Schneider, H. Toufar, A. Samoson, D. Freude, Solid State Nucl. Magn. Reson. **35**, 87 (2009)
32. H. Guesmi, P. Massiani, H. Nouali, J.L. Paillaud, Microporous Mesoporous Mater. **159**, 87 (2012)
33. G.H. Kuhl, Zeolites **7**, 451 (1987)
34. M. Iwama, Y. Suzuki, J. Plévert, K. Itabashi, M. Ogura, T. Okubo, Cryst. Growth Des. **10**, 3471 (2010)
35. G. Xiong, Y. Yu, Z. Feng, Q. Xin, F.S. Xiao, C. Li, Microporous Mesoporous Mater. **42**, 317 (2001)
36. F. Fan, Z. Feng, G. Li, K. Sun, P. Ying, C. Li, Chem. Eur. J. **14**, 5125 (2008)
37. F. Fan, Z. Feng, C. Li, Chem. Soc. Rev. **39**, 4794 (2010)
38. A. Depla, E. Verheyen, A. Veyfeyken, E. Gobechiya, T. Hartmann, R. Schaefer, J.A. Martens, C.E.A. Kirschhock, Phys. Chem. Chem. Phys. **13**, 13730 (2011)
39. B. Lok, T. Cannan, C. Messina, Zeolites **3**, 282 (1983)
40. S. Le Caér, F. Brunet, C. Chatelain, D. Durand, V. Dauvois, T. Charpentier, JPh Renault, J. Phys. Chem. C **116**, 4748 (2012)
41. K. Eichele, R.E. Wasylishen, v. 1.19.15 edn. (2009)
42. A. Inayat, I. Knoke, E. Spiecker, W. Schwieger, Angew. Chem. Int. Ed. **51**, 1962 (2012)
43. P.K. Dutta, K.M. Rao, J.Y. Park, J. Phys. Chem. **95**, 6654 (1991)
44. P.K. Dutta, D. Shieh, M. Puri, Zeolites **8**, 306 (1988)
45. C. Bremard, M. Le Maire, J. Phys. Chem. **97**, 9695 (1993)
46. A. Miecznikowski, J. Hanuza, Zeolites **5**, 188 (1985)
47. J. Twu, P.K. Dutta, C.T. Kresge, Zeolites **11**, 672 (1991)
48. P.K. Dutta, D. Shieh, M.J. Puri, Phys. Chem. **91**, 2332 (1987)
49. P.K. Dutta, J. Twu, J. Phys. Chem. **95**, 2498 (1991)
50. W. Yan, X. Song, R. Xu, Microporous Mesoporous Mater. **123**, 50 (2009)
51. T. Cheng, J. Xu, X. Li, Y. Li, B. Zhang, W. Yan, J. Yu, H. Sun, F. Deng, R. Xu, Microporous Mesoporous Mater. **152**, 190 (2012)
52. P. Bodart, J.B. Nagy, Z. Gabelica, E.G. Derouane, J. Chim. Phys. **83**, 777 (1986)
53. L. Ren, C. Li, F. Fan, Q. Guo, D. Liang, Z. Feng, C. Li, S. Li, F.S. Xiao, Chem. Eur. J. **17**, 6162 (2011)
54. C. Doremieux-Morin, C. Martin, J.M. Bregeault, J. Fraissard, Appl. Catal. **77**, 149 (1991)
55. G.E. Maciel, C.E. Bronnimann, R.C. Zeigler, I.S. Chuang, D.R. Kinney, E.A. Keiter, Adv. Chem. Ser. **234**, 269 (1994)
56. C.C. Liu, G.E. Maciel, J. Am. Chem. Soc. **118**, 5103 (1996)
57. M. Ogura, Y. Kawazu, H. Takahashi, T. Okubo, Chem. Mater. **15**, 2661 (2003)
58. E. Lippmaa, M. Maegi, A. Samoson, M. Tarmak, G. Engelhardt, J. Am. Chem. Soc. **103**, 4992 (1981)
59. H. Koller, G. Engelhardt, A.P.M. Kentgens, J. Sauer, J. Phys. Chem. **98**, 1544 (1994)
60. I. Hannus, I. Kiricsi, P. Lentz, J. Nagy, Colloids Surf. A **158**, 29 (1999)
61. A. Seidel, U. Tracht, B. Boddenberg, J. Phys. Chem. **100**, 15917 (1996)
62. I.L. Moudrakovski, J.A. Ripmeester, J. Phys. Chem. B **111**, 491 (2007)
63. A.T. Durant, K.J. MacKenzie, H. Maekawa, Dalton Trans. **40**, 4865 (2011)
64. V.F. Barbosa, K.J. MacKenzie, Mater. Lett. **57**, 1477 (2003)
65. M. Smith, Clays Clay Miner. **40**, 253 (1992)